Observability Analysis of Receiver Localization via Pseudorange Measurements From a Single LEO Satellite

Ralph Sabbagh, *Student Member, IEEE*, and Zaher M. Kassas, *Senior Member, IEEE*

***Abstract*—This letter presents an observability analysis for terrestrial receiver localization via pseudorange measurements extracted from a single low Earth orbit (LEO) satellite. It is shown that a stationary receiver with an unknown state (position and time) can theoretically localize itself with a LEO satellite with a known state (position, velocity, and time). In addition, bounds on the determinant of the *l*-step observability matrix are derived and geometric interpretations are presented indicating directions of poor observability. The implications of the analysis on observability-aided LEO satellite selection are discussed. Experimental results are presented showcasing the conclusions of the observability analysis for a receiver localizing itself with a single Starlink satellite or a single Orbcomm satellite.**

***Index Terms*—Observability analysis, satellite selection, low Earth orbit, Starlink, Orbcomm.**

I. Introduction

THE ADVENT of low Earth orbit (LEO) satellite mega-constellations promises to revolutionize several domains, bringing unprecedented high-resolution images; remote sensing; and global, high-availability, high-bandwidth, and low-latency Internet [1]. Due to LEO satellites' inherently desirable attributes, namely: (i) geometric and spectral diversity, (ii) abundance, (iii) high received signal power, and (iv) high orbital velocity, LEO satellites offer an attractive alternative to global navigation satellite systems (GNSS), which reside in medium Earth orbit (MEO) [2], [3].

The promise of utilizing LEO satellites for navigation has been the subject of recent theoretical and experimental studies [4], [5]. In [6], a generalized geometric dilution of precision (GDOP) analysis was presented that used Doppler shifts extracted from eight or more LEO satellites to localize a receiver via a static estimator. In [7], an adaptive Kalman filter was developed, achieving the first carrier phase tracking and positioning results using six Starlink LEO satellites.

LEO satellites orbit the Earth at much higher rates than GNSS satellites. Contrast, for example, the orbital period of a GPS MEO satellite (11 hr, 58 min) with that of Orbcomm LEO satellites (about 99 min) and Starlink LEO satellites (about 96 min). This yields significant change in their geometry, which can be exploited to localize a terrestrial receiver with fewer satellites. In particular, while four GNSS satellites are needed to estimate the states of the receiver via a static estimator (e.g., nonlinear least squares), a single LEO satellite can be used to localize the receiver via a dynamic estimator (e.g., an extended Kalman filter (EKF)) by fusing consecutive LEO measurements taken over a relatively short period of time. A few studies demonstrating the impact of receiver localization using a small number of satellites have been conducted in the literature. In [8], pseudorange and Doppler measurements were combined for stationary receiver positioning using two and three satellites without the use of a base station or differential positioning techniques.

Observability analysis with LEO satellites has been studied in the context of space situational awareness with relative position measurements [9] and orbit determination with angles-only measurements [10]. Moreover, observability of *planar* environments comprising terrestrial transmitters with unknown positions and time have been studied in [11], where estimability was *numerically* assessed from the EKF's estimation error covariance, and in [12], where the Riccati equation was analyzed to conclude that *simultaneously* estimating the receiver's and transmitter's time is stochastically unobservable. However, observability analysis with a small number of LEO satellites in the context of localization has not been thoroughly studied. This letter analyzes the observability of *three-dimensional* receiver localization via pseudorange measurements extracted from the signals of a single LEO satellite. It is shown that a stationary receiver with an unknown state (position and time) can theoretically localize itself with a LEO satellite with a known state (position, velocity, and time). In addition, *analytical* bounds on the determinant of the *l*-step observability matrix are derived indicating directions of poor observability. It is concluded that the system becomes unobservable if the receiver is in the satellite's orbital plane or along the normal to the satellite's orbital plane. The implications of the analysis

Manuscript received 21 March 2022; revised 25 May 2022; accepted 17 June 2022. Date of publication 30 June 2022; date of current version 15 September 2022. This work was supported in part by the National Science Foundation (NSF) under Grant 1929965 and Grant 1929571, and in part by the U.S. Department of Transportation (USDOT) for the CARMEN University Transportation Center (UTC) under Grant 69A3552047138. Recommended by Senior Editor V. Ugrinovskii. *(Corresponding author: Zaher M. Kassas.)*

Ralph Sabbagh is with the Department of Mechanical and Aerospace Engineering, University of California, Irvine, CA 92697 USA (e-mail: rsabbag1@uci.edu).

Zaher M. Kassas is with the Department of Electrical and Computer Engineering, The Ohio State University, Columbus, OH 43210 USA (e-mail: zkassas@ieee.org).

Digital Object Identifier 10.1109/LCSYS.2022.3187522

on observability-aided LEO satellite selection are discussed, where the presented surface plots of the observability matrix can aid in selecting the satellite with desired (i) visibility duration, (ii) elevation profile, and (iii) altitude and relative orbital inclination angle. Experimental results are presented showcasing the conclusions of the observability analysis for a receiver localizing itself with a single Starlink satellite or a single Orbcomm satellite.

This letter is structured as follows. Section II describes the dynamics and measurement models. Section III analyzes analytically the observability of receiver localization using pseudorange measurements from a single LEO satellite and gives geometric interpretations of the derived results. Section IV presents experimental results with Orbcomm and Starlink LEO satellites, demonstrating the implications of the observability analysis on the estimation performance.

II. Preliminaries and Model Description

A. Observability of LTV Systems

Consider the discrete-time (DT) linear time-varying (LTV) dynamical system Σ given by

$$\Sigma : \begin{cases} \boldsymbol{x}(k+1) = \mathbf{F}(k)\,\boldsymbol{x}(k) + \mathbf{G}(k)\,\boldsymbol{u}(k), \\ \boldsymbol{y}(k) = \mathbf{H}(k)\,\boldsymbol{x}(k), \end{cases} \tag{1}$$

where $\boldsymbol{x} \in \mathbb{R}^n$, $\boldsymbol{u} \in \mathbb{R}^p$, and $\boldsymbol{y} \in \mathbb{R}^q$ are the system state, input, and measurement vectors at time-step k, respectively, and $k \in \mathbb{N}$. The state transition matrix corresponding to Σ from time-step j to time-step i is given by

$$\Phi(i,j) \triangleq \begin{cases} \mathbf{F}(i-1)\,\mathbf{F}(i-2)\cdots\mathbf{F}(j), & \text{if } i > j, \\ \mathbf{I}_{n\times n}, & \text{if } i = j, \end{cases}$$

where $\mathbf{I}_{n\times n}$ denotes an $n \times n$ identity matrix. The following theorem characterizes the observability of DT LTV systems via the l-step observability matrix [13].

Theorem 1: The DT LTV system (1) is l-step observable if and only if its corresponding l-step observability matrix

$$\mathcal{O}(k, k+l-1) \triangleq \begin{bmatrix} \mathbf{H}(k)\,\Phi(k,k) \\ \mathbf{H}(k+1)\,\Phi(k+1,k) \\ \vdots \\ \mathbf{H}(k+l-1)\,\Phi(k+l-1,k) \end{bmatrix}, \tag{2}$$

is full rank. Theorem 1 can be applied to nonlinear systems by linearizing at each time-step k around $\boldsymbol{x}(k)$. The achieved observability results therein will only be valid locally [14].

B. Receiver Dynamics

The terrestrial receiver's position $\boldsymbol{r}_r \in \mathbb{R}^3$ is assumed to be fixed in the Earth-centered inertial (ECI) frame and its distance from the center of Earth is denoted by $r = \|\boldsymbol{r}_r\|_2$. The dynamics of the receiver's clock error states (i.e., bias δt_r and drift $\dot{\delta t}_r$) is modeled as a double integrator driven by process noise [15]. The receiver's dynamics is then given by

$$\boldsymbol{x}_r(k+1) = \mathbf{F}_r\,\boldsymbol{x}_r(k) + \boldsymbol{w}_r(k),$$

where $\boldsymbol{x}_r \triangleq \left[\boldsymbol{r}_r^\mathsf{T},\ c\,\delta t_r,\ c\,\dot{\delta t}_r\right]^\mathsf{T}$ is the receiver's state vector, c denotes the speed of light, and $\boldsymbol{w}_r$ is a process noise modeled as a zero-mean white random sequence with covariance $\mathbf{Q}_r = \mathrm{diag}[\mathbf{0}_{3\times3},\ \mathbf{Q}_{cr}]$. The receiver state matrix is given by

$$\mathbf{F}_r = \begin{bmatrix} \mathbf{I}_{3\times3} & \mathbf{0}_{3\times2} \\ \mathbf{0}_{2\times3} & \mathbf{F}_{\text{clk}} \end{bmatrix}, \quad \mathbf{F}_{\text{clk}} = \begin{bmatrix} 1 & T \\ 0 & 1 \end{bmatrix},$$

where T is the sampling period. In this letter, the simplest receiver dynamics was considered to focus on the change in geometry due to the moving satellite. More elaborate receiver dynamics could be considered in future work.

C. LEO Satellite Dynamics

The LEO satellite is assumed to follow a circular Keplerian orbit with fixed inclination and a prescribed orbital radius denoted by $a = \|\boldsymbol{r}_s(t)\|_2$ where $0 < r < a$. Under the action of Earth's gravitational field, the satellite's orbital dynamics in continuous-time will be assumed to follow a simplified two-body model given by

$$\ddot{\boldsymbol{r}}_s(t) = -\frac{\mu}{a^3}\,\boldsymbol{r}_s(t) + \boldsymbol{w}_s(t), \tag{3}$$

where $\boldsymbol{r}_s \in \mathbb{R}^3$ is the satellite's position in the ECI frame and $\boldsymbol{w}_s$ is a process noise vector of acceleration perturbations resulting from Earth's non-uniform gravitational potential, atmospheric drag, solar radiation pressure, gravitational pull of other celestial bodies, and general relativity [16]. The following constraints on the satellite dynamics hold $\forall\, t > 0$

$$\begin{aligned} \langle \boldsymbol{r}_s(t), \boldsymbol{r}_s(t) \rangle &= a^2, \\ \langle \dot{\boldsymbol{r}}_s(t), \dot{\boldsymbol{r}}_s(t) \rangle &= \alpha^2\, a^2, \\ \langle \boldsymbol{r}_s(t), \dot{\boldsymbol{r}}_s(t) \rangle &= 0, \end{aligned}$$

where $\alpha^2 \triangleq \mu/a^3$. The dynamics of the satellite's clock bias δt_s and drift $\dot{\delta t}_s$ are modeled similarly to the receiver's clock error dynamics [15]. Next, the satellite dynamics in (3) can be discretized at a sampling period T to yield

$$\boldsymbol{x}_s(t_{k+1}) = \mathbf{F}_s\,\boldsymbol{x}_s(t_k) + \boldsymbol{w}_s(t_k),$$

where $\boldsymbol{x}_s = [\boldsymbol{r}_s^\mathsf{T},\ \dot{\boldsymbol{r}}_s^\mathsf{T},\ c\,\delta t_s,\ c\,\dot{\delta t}_s]^\mathsf{T}$ is the satellite's state vector and $\boldsymbol{w}_s$ is a process noise modeled as a zero-mean white random sequence with covariance $\mathbf{Q}_s$, and $\mathbf{F}_s$ is given by

$$\mathbf{F}_s = \begin{bmatrix} \cos(\alpha T)\,\mathbf{I}_{3\times3} & (1/\alpha)\,\sin(\alpha T)\,\mathbf{I}_{3\times3} & \mathbf{0}_{3\times2} \\ -\alpha\,\sin(\alpha T)\,\mathbf{I}_{3\times3} & \cos(\alpha T)\,\mathbf{I}_{3\times3} & \mathbf{0}_{3\times2} \\ \mathbf{0}_{2\times3} & \mathbf{0}_{2\times3} & \mathbf{F}_{\text{clk}} \end{bmatrix}.$$

D. Measurement Model

The pseudorange measurement extracted by the receiver from the satellite signals at time-step k, after compensating for ionospheric and tropospheric delays [3], is modeled as

$$\rho(k) = \|\boldsymbol{r}_r - \boldsymbol{r}_s(k')\|_2 + c\left(\delta t_r(k) - \delta t_s(k')\right) + \nu(k), \tag{4}$$

where k' represents discrete-time $t_k = k\,T - \delta t_{TOF}$ with δt_{TOF} being the transmission delay of the signal. The term ν is the measurement noise, which is modeled as a zero-mean white Gaussian sequence with variance σ^2.

III. Observability Analysis

This section analyzes the observability of receiver localization with a single LEO satellite under two scenarios. The first scenario considers a receiver with *unknown* position states but *known* clock error states. Results from this simple scenario will serve as a stepping stone towards the second scenario, which considers a receiver with *unknown* position states and *unknown* clock error states. In each scenario, the satellite's states are assumed to be known, which is the case whenever (i) a satellite transmits its ephemeris and clock errors (e.g., Orbcomm satellites transmit their states, estimated from onboard GPS receivers [3]) or (ii) an estimator is employed to estimate the LEO satellite's states (e.g., via a differential navigation framework utilizing a known base receiver [17] or via a simultaneous tracking and navigation (STAN) framework [3]). It is worth noting that instead of estimating the receiver's clock error states, the following analysis readily extends to the case of estimating the *difference* between the receiver's and LEO satellite's clock error states, $\Delta\delta t \triangleq \delta t_r - \delta t_s$ and $\Delta\dot{\delta} t \triangleq \dot{\delta} t_r - \dot{\delta} t_s$, which could be desirable for stochastic observability considerations [12]. The nonlinear pseudorange measurement (4) is linearized at time-step k with respect to the unknown receiver states and the corresponding Jacobian matrix is used to build the l-step observability matrix. The scenarios are summarized below

- *Scenario 1:* A stationary receiver with *unknown position states* but *known clock error states* makes pseudorange measurements to a LEO satellite with *known states*. The measurement Jacobian is given by $\mathbf{H}(k) = \boldsymbol{l}_k^{\mathsf{T}}$.
- *Scenario 2:* A stationary receiver with *unknown position states and clock error states* makes pseudorange measurements to a LEO satellite with *known states*. The measurement Jacobian is given by $\mathbf{H}(k) = \begin{bmatrix}\boldsymbol{l}_k^{\mathsf{T}} & 1 & 0\end{bmatrix}$.

Above, $\boldsymbol{l}_k \in \mathbb{R}^3$ denotes the unit line-of-sight (LOS) vector between the receiver and satellite at time-step k, given by

$$\boldsymbol{l}_k \triangleq \frac{\boldsymbol{r}_r - \boldsymbol{r}_s(k)}{\|\boldsymbol{r}_r - \boldsymbol{r}_s(k)\|_2}.$$

In what follows, the l-step observability of the aforementioned scenarios is investigated, and bounds on the determinants of observability matrices therein are derived.

A. Scenario 1: Pseudorange Measurements With Unknown Receiver Position States But Known Clock Error States

In this scenario, the only unknown states are the receiver's position, and the 3-step observability matrix is given by

$$\mathcal{O}(k, k+2) = \begin{bmatrix}\boldsymbol{l}_k & \boldsymbol{l}_{k+1} & \boldsymbol{l}_{k+2}\end{bmatrix}^{\mathsf{T}}, \tag{5}$$

where the transition matrix $\Phi = \mathbf{I}_{3\times 3}$ and the measurement Jacobian $\mathbf{H}(k) = l_k^{\mathsf{T}}$ are used to build $\mathcal{O}(k, k+2)$. Let $\mathcal{O}(k, k+2) \triangleq \mathcal{O}_3$. An expression for $\det(\mathcal{O}_3)$ is derived as a function of the relative geometry between the receiver and the satellite.

Theorem 2: Let $c_n \triangleq \cos(\alpha n T)$, $s_n \triangleq \sin(\alpha n T)$, and

$$\beta^k \triangleq \frac{1}{\|\Delta\boldsymbol{r}(k)\|_2 \, \|\Delta\boldsymbol{r}(k+1)\|_2 \, \|\Delta\boldsymbol{r}(k+2)\|_2},$$

where $\Delta\boldsymbol{r}(k) \triangleq \boldsymbol{r}_r - \boldsymbol{r}_s(k)$. The determinant of the 3-step observability matrix in (5) is given by

$$\det(\mathcal{O}_3) = \beta^k \, (2\, s_1 - s_2)\, a^2 \, r \, \sin(\theta), \tag{6}$$

where θ is the angle between the receiver's position vector $\boldsymbol{r}_r$ and the orbital plane of the LEO satellite.

Proof: Since $\mathcal{O}_3$ is a 3×3 matrix, its determinant is equal to the scalar triple product of its rows which are given by the unit LOS vectors $\boldsymbol{l}_k$, $\boldsymbol{l}_{k+1}$, and $\boldsymbol{l}_{k+2}$ as follows

$$\begin{aligned}\det(\mathcal{O}_3) &= \boldsymbol{l}_k \cdot (\boldsymbol{l}_{k+1} \times \boldsymbol{l}_{k+2}) \\ &= \beta^k \, \Delta\boldsymbol{r}(k) \cdot (\Delta\boldsymbol{r}(k+1) \times \Delta\boldsymbol{r}(k+2)),\end{aligned} \tag{7}$$

where the terms $r_s(k+1)$ in $\Delta r(k+1)$ and $r_s(k+2)$ in $\Delta r(k+2)$ can be written in terms of $r_s(k)$ and $\dot{r}_s(k)$ using the satellite dynamics $\mathbf{F}_s$ defined in Section II-C as follows

$$\Delta\boldsymbol{r}(k+1) = \boldsymbol{r}_r - c_1 \, \boldsymbol{r}_s(k) - \frac{1}{\alpha} s_1 \, \dot{\boldsymbol{r}}_s(k), \tag{8}$$

$$\Delta\boldsymbol{r}(k+2) = \boldsymbol{r}_r - c_2 \, \boldsymbol{r}_s(k) - \frac{1}{\alpha} s_2 \, \dot{\boldsymbol{r}}_s(k). \tag{9}$$

Plugging (8) and (9) in (7) yields

$$\begin{aligned}\det(\mathcal{O}_3) &= \frac{\beta^k \, (2\, s_1 - s_2)}{\alpha} \left(\boldsymbol{r}_r \cdot (\boldsymbol{r}_s(k) \times \dot{\boldsymbol{r}}_s(k))\right) \\ &= \beta^k \, (2\, s_1 - s_2)\, a^2 \, r \, \sin(\theta).\end{aligned}$$

■

Hereafter, θ is referred to as the *relative orbital inclination angle* between the receiver and the LEO satellite. Ideally, θ is assumed constant for a stationary receiver during the time window through which it is seeing a LEO satellite. In what follows, time-independent bounds on $\det(\mathcal{O}_3)$ are derived.

Corollary 1: The determinant of the 3-step observability matrix in (5) can be bounded as follows

$$0 \le L(\theta) \le \det(\mathcal{O}_3) \le U(\theta),$$

$$L(\theta) = \frac{(2\, s_1 - s_2)\, a^2 \, r \, \sin(\theta)}{\left(a^2 + r^2 + 2\, a\, r \, \cos(\theta)\right)^{3/2}},$$

$$U(\theta) = \frac{(2\, s_1 - s_2)\, a^2 \, r \, \sin(\theta)}{\left(a^2 + r^2 - 2\, a\, r \, \cos(\theta)\right)^{3/2}},$$

where $0 \le \theta \le \pi/12$ and $0 \le \alpha \, k \, T \le \pi/6$ for all $k \in \mathbb{N}$.

Proof: Using the law of cosines, the minimum and maximum Euclidean distances between the receiver and the satellite; denoted by d_{min} and d_{max}, respectively, are given by

$$\min_{k\in\mathbb{N}} \|\boldsymbol{r}_r - \boldsymbol{r}_s(k)\|_2 = \left(a^2 + r^2 - 2\, a\, r \, \sin(\theta)\right)^{1/2}, \tag{10}$$

$$\max_{k\in\mathbb{N}} \|\boldsymbol{r}_r - \boldsymbol{r}_s(k)\|_2 = \left(a^2 + r^2 + 2\, a\, r \, \sin(\theta)\right)^{1/2}, \tag{11}$$

such that $d_{max}^{-3} \le \beta^k \le d_{min}^{-3}$ for all $k \in \mathbb{N}$. ■

The inequalities on θ and $\alpha \, k \, T$ are placed with the understanding that a LEO satellite should be visible for a long enough time to provide useful measurements. Next, observability results and geometric interpretations are deduced.

Proposition 1: If the receiver is in the orbital plane of the LEO satellite, the system is not l-step observable.

Proof: If the receiver is in the orbital plane of the LEO satellite, then $\theta = 0$. This implies that $U(\theta) = U(0) = 0$. As a result, $\det(\mathcal{O}_3) = 0$ and $\mathcal{O}_3$ is rank deficient. In fact, the rows of $\mathcal{O}_l$, which represent consecutive unit LOS vectors tracing the satellite's orbit, are coplanar lying in the orbital plane of the satellite. As a result, $\text{rank}[\mathcal{O}_l] \le 2$, for all $l \ge 2$. ■

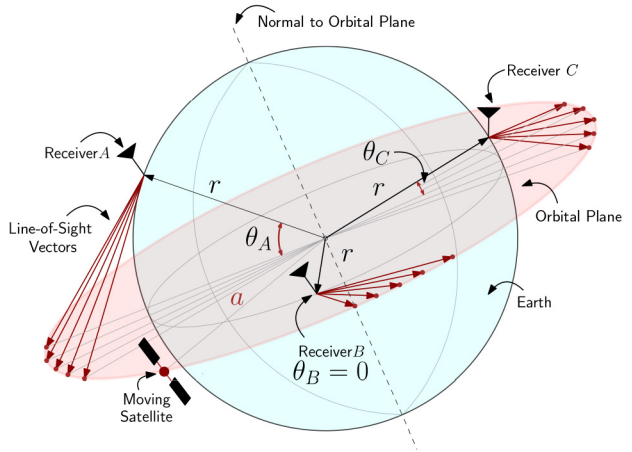

Fig. 1. Comparison between the geometric diversity of the LOS vectors based on the relative orbital inclinations θ_A, θ_B, and θ_C ($\theta_A \gg \theta_C \gg \theta_B$) created between the LEO satellite and receivers *A*, *B*, and *C*, respectively. Receiver *A* makes LOS measurements that are relatively closer to each other compared to receiver *C* (large θ), and receiver *B* makes LOS measurements that are coplanar in the orbital plane of the LEO satellite (small θ).

Remark 1: The unobservable subspace in the case above is spanned by the normal to the satellite's orbital plane, otherwise known as the satellite's cross direction. This implies that initial receiver position states along this direction are indistinguishable. The impact of this on localization using a single overhead LEO satellite is demonstrated in Section IV.

Proposition 2: If the receiver is not in the orbital plane of the LEO satellite, the system is l-step observable for $l \geq 3$.

Proof: If the receiver is not in the orbital plane of the LEO satellite, then $\theta \neq 0$. As a result, $L(\theta) > L(0) > 0$, and $\det(\mathcal{O}_3) \neq 0$ with $\text{rank}[\mathcal{O}_l] = 3$, for all $l \geq 3$. In fact, the rows of $\mathcal{O}_l$, which represent consecutive unit LOS vectors tracing the satellite's orbit, are no longer coplanar. This implies that the corresponding scalar triple product of any three consecutive unit LOS vectors is nonzero within a single orbital period. ∎

The above analysis and (6) show that the size of θ normalized by the cube of the receiver-satellite range can measure how close the l-step observability matrix is to singularity ($\det(\mathcal{O}_3) \propto \beta^k \sin(\theta)$). As a result, a relationship between the singularity of $\mathcal{O}_3$ and the geometric diversity of the unit LOS vectors can be established. Namely, for small θ, the receiver is near the orbital plane of the satellite so that the LOS vectors are almost *coplanar*. For large θ, the receiver is far enough from the satellite so that the LOS vectors are almost *collinear*. In both extremes, the LOS vectors have poor geometric diversity. An exaggerated comparison illustrating the impact of θ on the geometric diversity of the LOS vectors is shown in Fig. 1, where three receiver positions resulting in three drastically different values of θ result in LOS vectors with varying geometric diversity. A study on the singularity of $\mathcal{O}_3$ is shown in Fig. 2(a), where the values of $\det(\mathcal{O}_3)$ were computed from simulated LOS vectors created between a stationary receiver and a satellite traveling along a circular orbit at an altitude of 521 km (computations were repeated for varying values of $\theta \in [0,\ \pi/12]$). It is observed that $\det(\mathcal{O}_3)$ drastically diminishes for θ values which are too small or too large, implying that a "favorable" relative orbital inclination region (shown in

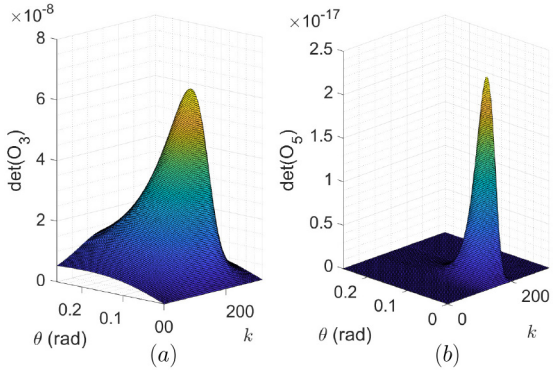

Fig. 2. Values of $\det(\mathcal{O}_3)$ (left) and $\det(\mathcal{O}_5)$ (right) computed for different values of θ in radians at each time-step k.

Fig. 2 in yellow) lying in between the two extremes exists where $\det(\mathcal{O}_3)$ is maximal over the navigation window of the receiver. Implications of this on observability-based satellite selection is discussed in Section IV.

B. Scenario 2: Pseudorange Measurements With Unknown Receiver Position States and Unknown Clock Error States

In this scenario, the receiver state is unknown, and the 5-step observability matrix is given by

$$\mathcal{O}(k, k+4) = \begin{bmatrix} \boldsymbol{l}_k & \boldsymbol{l}_{k+1} & \boldsymbol{l}_{k+2} & \boldsymbol{l}_{k+3} & \boldsymbol{l}_{k+4} \\ 1 & 1 & 1 & 1 & 1 \\ 0 & T & 2T & 3T & 4T \end{bmatrix}^{\mathsf{T}}, \quad (12)$$

where the transition matrix $\Phi = \mathbf{F}_r \in \mathbb{R}^{5\times5}$ and the measurement Jacobian $\mathbf{H}(k) = [\boldsymbol{l}_k^{\mathsf{T}} \quad 1 \quad 0] \in \mathbb{R}^{1\times5}$ are used to build $\mathcal{O}(k, k+4)$. Let $\mathcal{O}(k, k+4) \triangleq \mathcal{O}_5$. Next, an expression for $\det(\mathcal{O}_5)$ is derived as a function of the relative geometry between the receiver and the satellite.

Proposition 3: Let m, n, and $p \in \mathbb{N}$ with $m < n < p$, then the following equality holds

$$\boldsymbol{l}_m \cdot (\boldsymbol{l}_n \times \boldsymbol{l}_p) = \gamma_{mnp}\, \beta_{mnp}^k\, a^2\, r\, \sin(\theta),$$

where the scalars $\gamma_{mnp} > 0$ and $\beta_{mnp}^k > 0$ are given by

$$\gamma_{mnp} \triangleq s_{n-m} + s_{p-n} - s_{p-m},$$
$$\beta_{mnp}^k \triangleq \frac{1}{\|\Delta\boldsymbol{r}(k+m)\|_2\, \|\Delta\boldsymbol{r}(k+n)\|_2\, \|\Delta\boldsymbol{r}(k+p)\|_2},$$

where $0 \leq \theta \leq \pi/12$ and $0 \leq \alpha\, k\, T \leq \pi/6$ for all $k \in \mathbb{N}$.

Proof: The proof proceeds similarly to that of Theorem 2. ∎

Theorem 3: The determinant of the 5-step observability matrix in (12) is given by

$$\det(\mathcal{O}_5) = T\,(a_1 - a_2 + a_3 - a_4)\, a^2\, r\, \sin(\theta), \quad (13)$$

where a_1, a_2, a_3, and a_4 are scalars given by

$$a_1 = \gamma_{012}\,(\beta_{012}^k + \beta_{234}^k) + \gamma_{014}\,(\beta_{014}^k + \beta_{034}^k),$$
$$a_2 = 2\left(\gamma_{013}\,\beta_{013}^k + \gamma_{024}\,\beta_{024}^k + \gamma_{134}\,\beta_{134}^k\right),$$
$$a_3 = 3\,\gamma_{023}\left(\beta_{023}^k + \beta_{124}^k\right),$$
$$a_4 = 4\,\gamma_{123}\,\beta_{123}^k.$$

Proof: The determinant of $\mathcal{O}_5$ can be expressed in terms of a product of determinants involving block partitions of $\mathcal{O}_5$ via the Schur complement formula as follows

$$\det(\mathcal{O}_5) = \det(\mathbf{D})\,\det(\mathbf{A} - \mathbf{B}\mathbf{D}^{-1}\mathbf{C}), \tag{14}$$

where the matrices $\mathbf{A}$, $\mathbf{B}$, $\mathbf{C}$, and $\mathbf{D}$ are given by

$$\mathbf{A} = \begin{bmatrix} \boldsymbol{l}_k & \boldsymbol{l}_{k+1} & \boldsymbol{l}_{k+2} \end{bmatrix}^{\mathsf{T}},\ \mathbf{B} = \begin{bmatrix} 1 & 1 & 1 \\ 0 & T & 2T \end{bmatrix}^{\mathsf{T}},$$

$$\mathbf{C} = \begin{bmatrix} \boldsymbol{l}_{k+3} & \boldsymbol{l}_{k+4} \end{bmatrix}^{\mathsf{T}},\ \text{and}\ \mathbf{D} = \begin{bmatrix} 1 & 1 \\ 3T & 4T \end{bmatrix}^{\mathsf{T}}.$$

Plugging the above expressions for matrices $\mathbf{A}$, $\mathbf{B}$, $\mathbf{C}$, and $\mathbf{D}$ in equation (14) and expanding yields

$$\det(\mathcal{O}_5) = T \begin{vmatrix} \boldsymbol{l}_k^{\mathsf{T}} - 4\boldsymbol{l}_{k+3}^{\mathsf{T}} + 3\boldsymbol{l}_{k+4}^{\mathsf{T}} \\ \boldsymbol{l}_{k+1}^{\mathsf{T}} - 3\boldsymbol{l}_{k+3}^{\mathsf{T}} + 2\boldsymbol{l}_{k+4}^{\mathsf{T}} \\ \boldsymbol{l}_{k+2}^{\mathsf{T}} - 2\boldsymbol{l}_{k+3}^{\mathsf{T}} + \boldsymbol{l}_{k+4}^{\mathsf{T}} \end{vmatrix}.$$

Hence, $\det(\mathcal{O}_5)$ is now expressed in terms of the determinant of a 3×3 matrix which is equal to the scalar triple product of its rows. By expanding this product, the resulting terms can be grouped using Proposition 3, resulting in (13). ■

Time-independent bounds on $\beta^k_{m,n,p}$ can be derived as in the proof of Corollary 1, so that $d_{max}^{-3} \leq \beta^k_{mnp} \leq d_{min}^{-3}$ for all k, m, n, and $p \in \mathbb{N}$. Bounds on $\det(\mathcal{O}_5)$ are presented next.

Corollary 2: The determinant of the 5-step observability matrix in (13) can be bounded as follows

$$L(\theta) \leq \det(\mathcal{O}_5) \leq U(\theta),$$

$$L(\theta) = 16\, s_1^3\,(1 - c_1)\, a^2\, r\, T \left(\frac{1}{d_{max}^3} - \frac{1}{d_{min}^3} \right) \sin(\theta),$$

$$U(\theta) = 16\, s_1^3\,(1 - c_1)\, a^2\, r\, T \left(\frac{1}{d_{min}^3} - \frac{1}{d_{max}^3} \right) \sin(\theta),$$

where $0 \leq \theta \leq \pi/12$ and $0 \leq \alpha\, k\, T \leq \pi/6$ for all $k \in \mathbb{N}$.

Proof: The proof proceeds similarly to that of Corollary 1. ■

Based on Theorem 3 and Corollary 2, the following observability results and geometric interpretations are deduced.

Proposition 4: If the receiver is in the orbital plane of the satellite or along the normal to the orbital plane of the satellite, the system is not l-step observable.

Proof: By construction, unobservable directions in Scenario I are inherited into Scenario II where additional receiver states are now unknown. Furthermore, if the receiver is along the normal to the orbital plane of the satellite, the minimum and maximum Euclidean distances between the receiver and the LEO satellite become equal which results in $U(\theta) = U(\frac{\pi}{2}) = 0$ and $L(\theta) = L(\frac{\pi}{2}) = 0$, implying that $\det(\mathcal{O}_5) = 0$. In fact, since a constant distance is maintained between the receiver-satellite pair, the stationary receiver can no longer disambiguate between its initial clock bias and the initial range from the satellite, no matter how many pseudorange measurements it makes from that satellite. At best, a one-dimensional unobservable subspace of $\mathbb{R}^5$ is maintained, so that $\text{rank}[\mathcal{O}_l] \leq 4$, for all $l \geq 4$. ■

Proposition 5: If the receiver is not in the orbital plane of the satellite, nor along the normal to the satellite's orbital plane, the system is l-step observable for $l \geq 5$.

Proof: It is enough to show by contradiction that the matrix $\mathcal{O}_5$ in this setting is non-singular. To that end, assume that there exists a nontrivial vector $\boldsymbol{v} \in \mathbb{R}^5$ such that $\mathcal{O}_5 \cdot \boldsymbol{v} = \mathbf{0}_{5\times 1}$. By partitioning $\boldsymbol{v}$ such that $\boldsymbol{v} = [\boldsymbol{u}^{\mathsf{T}}\ \ s\ \ w]^{\mathsf{T}}$ where $\boldsymbol{u} \in \mathbb{R}^3$, $s \in \mathbb{R}$, one obtains the following system of 5 equations:

$$\begin{cases} \langle \boldsymbol{l}_k, \boldsymbol{u} \rangle = -s \\ \langle \boldsymbol{l}_{k+1}, \boldsymbol{u} \rangle = -s - T\,w \\ \langle \boldsymbol{l}_{k+2}, \boldsymbol{u} \rangle = -s - 2\,T\,w \\ \langle \boldsymbol{l}_{k+3}, \boldsymbol{u} \rangle = -s - 3\,T\,w \\ \langle \boldsymbol{l}_{k+4}, \boldsymbol{u} \rangle = -s - 4\,T\,w. \end{cases} \tag{15}$$

From (15), it follows that $\boldsymbol{u}$ must make either constant or linearly increasing angles with 5 consecutive unit LOS vectors tracing the satellite's circular Keplerian orbit. Since the receiver is not in the orbital plane of the satellite, any 3 vectors chosen from 5 consecutive unit LOS vectors within a single orbital period are non-coplanar. If in addition, the receiver is not along the normal to the orbital plane of the satellite, then the corresponding difference vectors between the 5 unit LOS vectors are not coplanar and with same length. This implies that $\boldsymbol{u}$ must be the trivial vector, concluding the proof. ■

The observability surface in Fig. 2(b) is significantly smaller compared to Fig. 2(a). This reflects poorer observability conditions and loss of information due to the addition of unknown receiver states to the system. Finally, while the unobservable subspaces discussed are of zero measure and assume an ideal setting (perfect knowledge of a circular satellite ephemeris, non-rotating spherical Earth, etc), in a real setting, the satellite's orbit will experience random perturbations such that a receiver localizing itself would not lie exactly along the derived unobservable subspaces. Despite this, Section IV will show that a receiver still fails to localize itself due to the unobservable direction derived in the ideal setting.

IV. Experimental Results

To demonstrate the conclusions of the observability analysis on receiver localization, an experiment was conducted whereby pseudorange measurements, extracted from carrier phase observables [7], [17], from one Starlink satellite and one Orbcomm satellite were used to localize a stationary receiver using an EKF for LEO satellite visibility durations of 74 and 317 seconds, respectively. The Starlink and Orbcomm satellites possess average relative orbital inclinations of $\theta = 0.01457$ rad and $\theta = 0.00410$ rad, respectively, indicating that the receiver is relatively close to being in their orbital planes during each navigation window. For both satellites, the analysis in Section III shows that the determinant of the corresponding observability matrices is expected to be small enough so that the directions normal to the LEO satellites' orbital planes become nearly unobservable. The objective of the experiment is therefore to demonstrate that receiver localization using near-overhead passing LEO satellites will suffer from poor information in the direction normal to the LEO satellite's orbital plane. This implies that any initial receiver position error in the direction along the normal to the LEO satellite's orbital plane will not reduce in the EKF, due to the observability matrix being nearly singular. For the Starlink satellite, the satellite's states were estimated according to the framework discussed in [7], which estimated the satellite's ephemeris via simplified general perturbation 4 (SGP4)

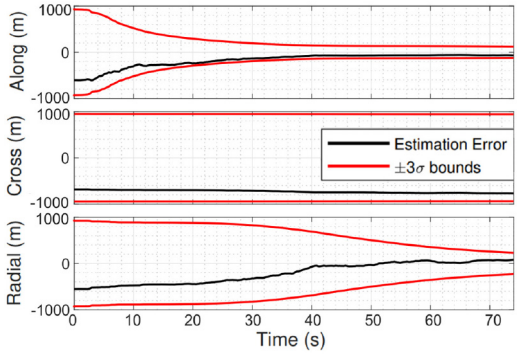

Fig. 3. Receiver position estimation errors resolved along the Starlink satellite body frame (in black) with $\pm 3\sigma$ bounds (in red).

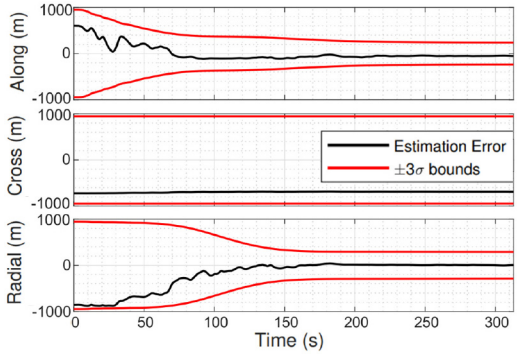

Fig. 4. Receiver position estimation errors resolved along the Orbcomm satellite body frame (in black) with $\pm 3\sigma$ bounds (in red).

TABLE I
RECEIVER LOCALIZATION ERROR

Satellite	Direction	Initial Error	Final Error
Starlink	Along (m)	-603.94	-67.14
	Cross (m)	-682.25	–768.41
	Radial (m)	-555.90	81.40
	Overall (m)	1,067.35	775.62
Orbcomm	Along (m)	604.47	-51.35
	Cross (m)	-722.25	-689.29
	Radial (m)	-856.47	7.79
	Overall (m)	1,273.30	691.24

orbit propagator initialized with two-line element (TLE) files. For the Orbcomm satellite, the satellite's states were obtained by decoding the downlink signal, which contains ephemeris and clock errors, estimated via the satellite's onboard GPS receivers [17]. The localization results are shown in Figs. 3 and 4, where the receiver's position estimation errors and the $\pm 3\sigma$-bounds are resolved along the LEO satellite's body frame (along-track, cross-track, and radial directions). Table I shows the initial and final receiver position estimation errors in each direction. It can be seen from Figs. 3 and 4 and Table I that while the receiver's position error in the along-track and radial directions decreases, there is no improvement in the cross-track direction. This confirms the observability result discussed in Section III, stating that the direction normal to the orbital plane of the satellite is unobservable for a receiver making measurements from incoming overhead satellites. Fig. 2 can be utilized for observability-based satellite selection to improve receiver localization. To this end, based on LEO satellite's SGP4-propagated TLE files, estimates for their respective altitudes as well as angles θ of their orbital planes with the receiver can be used to predict and select the satellite which will generate a navigation scenario which is most observable. Namely, given a set of LEO satellites, one can identify the one which will result in the best receiver localization performance, by taking into account the following criteria, which are all features of the observability surfaces shown in Fig. 2:

- The duration of time for which the satellite will be visible.
- The elevation profile of the satellite during this time.
- Satellite altitudes and relative orbital inclinations θ.

While the analysis in this letter considered a single LEO satellite, future work could generalize to multiple satellites and develop an observability-aided LEO satellite selection approach that determines the satellites that are expected to provide the best measurements for receiver localization.

REFERENCES

[1] S. Liu *et al.*, "LEO satellite constellations for 5G and beyond: How will they reshape vertical domains?" *IEEE Commun. Mag.*, vol. 59, no. 7, pp. 30–36, Jul. 2021.

[2] T. Reid *et al.*, "Navigation from low earth orbit—Part 1: Concept, current capability, and future promise," in *Position, Navigation, and Timing Technologies in the 21st Century*, vol. 2, J. Morton, F. van Diggelen, J. Spilker, Jr., and B. Parkinson, Eds. Hoboken, NJ, USA: Wiley-IEEE, 2021, ch. 43, pp. 1359–1379.

[3] Z. Kassas, "Navigation from low earth orbit—Part 2: Models, implementation, and performance," in *Position, Navigation, and Timing Technologies in the 21st Century*, vol. 2, J. Morton, F. van Diggelen, J. Spilker, Jr., and B. Parkinson, Eds. Hoboken, NJ, USA: Wiley-IEEE, 2021, ch. 43, pp. 1381–1412.

[4] Q. Wei, X. Chen, and Y. F. Zhan, "Exploring implicit pilots for precise estimation of LEO satellite downlink doppler frequency," *IEEE Commun. Lett.*, vol. 24, no. 10, pp. 2270–2274, Oct. 2020.

[5] S. Thompson, S. Martin, and D. Bevly, "Single Differenced doppler positioning with low earth orbit signals of opportunity and angle of arrival estimation," in *Proc. ION Int. Tech. Meeting*, 2020, pp. 497–509.

[6] M. Psiaki, "Navigation using carrier doppler shift from a LEO constellation: TRANSIT on steroids," *J. Inst. Navig.*, vol. 68, no. 3, pp. 621–641, Sep. 2021.

[7] J. Khalife, M. Neinavaie, and Z. Kassas, "The first carrier phase tracking and positioning results with starlink LEO satellite signals," *IEEE Trans. Aerosp. Electron. Syst.*, vol. 56, no. 2, pp. 1487–1491, Apr. 2022.

[8] E. Pike, F. van Graas, and S. Ugazio, "Two and three satellite positioning using doppler and pseudorange," in *Proc. Int. Tech. Meeting Inst. Navig.*, 2022, pp. 671–685.

[9] A. Friedman, "Observability analysis for space situational awareness," Ph.D. dissertation, Dept. Aeronaut. Astronaut., Purdue Univ., West Lafayette, IN, USA, 2020.

[10] E. Kaufman, T. Lovell, and T. Lee, "Nonlinear observability for relative orbit determination with angles-only measurements," *J. Astronaut. Sci.*, vol. 63, no. 1, pp. 60–80, 2016.

[11] Z. Kassas and T. Humphreys, "Observability and estimability of collaborative opportunistic navigation with pseudorange measurements," in *Proc. ION GNSS Conf.*, Sep. 2012, pp. 621–630.

[12] J. Morales and Z. Kassas, "Stochastic observability and uncertainty characterization in simultaneous receiver and transmitter localization," *IEEE Trans. Aerosp. Electron. Syst.*, vol. 55, no. 2, pp. 1021–1031, Apr. 2019.

[13] W. Rugh, *Linear System Theory*, 2nd ed. Upper Saddle River, NJ, USA: Prentice Hall, 1996.

[14] G. Huang, A. Mourikis, and S. Roumeliotis, "Observability-based rules for designing consistent EKF SLAM estimators," *Int. J. Robot. Res.*, vol. 29, no. 5, pp. 502–528, Apr. 2010.

[15] Y. Bar-Shalom, X. Li, and T. Kirubarajan, *Estimation With Applications to Tracking and Navigation*. New York, NY, USA: Wiley, 2002.

[16] O. Montenbruck and E. Gill, *Satellite Orbits: Models, Methods, and Applications*. Heidelberg, Germany: Springer, 2000.

[17] J. Khalife, M. Neinavaie, and Z. Kassas, "Navigation with differential carrier phase measurements from Megaconstellation LEO satellites," in *Proc. IEEE/ION Position Location Navig. Symp.*, Apr. 2020, pp. 1393–1404.